Letter

Generating symmetry-protected long-range entanglement

Shovan Dutta [1,2,3] Stefan Kuhr [4] and Nigel R. Cooper [1,5]

[1]*TCM Group, Cavendish Laboratory, University of Cambridge, JJ Thomson Avenue, Cambridge CB3 0HE, United Kingdom*
[2]*Max Planck Institute for the Physics of Complex Systems, 01187 Dresden, Germany*
[3]*Raman Research Institute, CV Raman Avenue, Sadashivanagar, Bangalore 560080, India*
[4]*Department of Physics, University of Strathclyde, Glasgow G4 0NG, United Kingdom*
[5]*Department of Physics and Astronomy, University of Florence, Via G. Sansone 1, 50019 Sesto Fiorentino, Italy*

(Received 7 February 2022; accepted 15 December 2023; published 23 February 2024)

Entanglement between spatially distant qubits is perhaps the most counterintuitive and vital resource for distributed quantum computing. However, despite a few special cases, there is no known general procedure to maximally entangle two distant parts of an interacting many-body system. Here we present a symmetry-based approach, whereby one applies several timed pulses to drive a system to a particular symmetry sector with maximal bipartite long-range entanglement. As a concrete example, we demonstrate how a simple sequence of on-site pulses on a qubit array can efficiently produce multiple stable nonlocal Bell pairs, realizable in present-day atomic and photonic experimental platforms. More generally, our approach paves a route for exotic state preparation by harnessing symmetry. For instance, we show how it allows the creation of long-sought-after superconducting η pairs in a repulsive Hubbard model.

DOI: 10.1103/PhysRevResearch.6.L012039

Introduction. Since the early days of quantum mechanics, entanglement has been seen as a fundamental quantum trait, which now lies at the heart of quantum information processing [1,2]. In recent decades, experiments have made great progress in generating entanglement between two isolated qubits via photon exchange [3–5] and combining such two-qubit gates to build multiqubit states [6–8]. However, it is much more challenging to entangle a pair of distant qubits in a system where multiple qubits interact with one another [9]. Theoretical protocols have largely focused on creating a single Bell pair between two ends of a spin chain [10–13]. Although more pairs can be entangled using specially designed nonuniform coupling [14,15] or correlated dissipation [16], these are seldom realized in experiments [17] and limited to free-fermionic chains.

Here, we introduce a more general approach that leverages the existence of a symmetry to create entanglement over increasingly long distances. As in classical mechanics, a symmetry in a quantum system is intimately linked to a conservation law, which divides the space of all states into decoupled sectors. We envision scenarios where these sectors can be characterized by increasing long-range entanglement, as in the examples below. Our idea is sketched in Fig. 1(a): Suppose the system is initially in some low-entangled state in sector $\mathcal{S}_0$, e.g., the ground state or a product state. We apply a series of symmetry-breaking pulses to drive the system toward the maximally entangled sector $\mathcal{S}_*$, hosting one or few states. The pulses are timed optimally to maximize this one-way transfer. If the transfer fidelity is high, one can produce a large weight in $\mathcal{S}_*$ with a small number of pulses.

We will show how this technique allows one to generate Bell pairs between any number of mirror-conjugate sites in a spin chain [Fig. 1(b)], realizing variants of the so-called "rainbow" state [18,19]. These states possess a high persistency of entanglement [20] and can be used to distribute entanglement in a quantum network [14]. They also arise in quantum many-body scars [21]. Unlike other protocols for creating rainbow-like states, we do not require the spin-spin interactions to be selectively driven [6,22], individually fine-tuned [14,15,18], or coupled with engineered dissipation [16,23,24]. Instead, our scheme uses local π pulses that are standard in experiments and works well even for a nonintegrable spin chain. The Bell pairs are created in a time linear in system size, and stable thereafter due to the symmetry conservation.

Furthermore, our approach extends, in principle, to arbitrary interacting systems with a similar symmetry structure. In particular, we show how one can drive a Fermi-Hubbard chain [25] toward an elusive maximally-correlated η-pairing state [26]. As the protocol is symmetry based, the entanglement generated is robust against any perturbation that preserves the symmetry.

Qubit-array protocol: Model. We consider the simplest spin-1/2 XX Hamiltonian with $2l+1$ sites for integer l,

$$\hat{H} = -(J/4)\sum_{i=-l}^{l-1}\left(\hat{\sigma}_i^x\hat{\sigma}_{i+1}^x + \hat{\sigma}_i^y\hat{\sigma}_{i+1}^y\right), \tag{1}$$

where the $\hat{\sigma}$'s are the Pauli spin operators and J is the spin-spin coupling ($\hbar = 1$). This model can be reduced to free fermions through a Jordan-Wigner (JW) map, $\hat{f}_i = \hat{\sigma}_i^- \prod_{j<i}(-\hat{\sigma}_j^z)$, where $\hat{\sigma}_i^{\pm} := (\hat{\sigma}_i^x \pm \mathrm{i}\hat{\sigma}_i^y)/2$ and $\hat{f}_i^\dagger$ creates

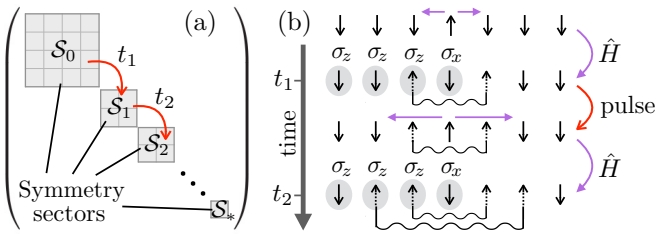

FIG. 1. (a) Schematic of how one can sequentially transfer a system through symmetry sectors $\mathcal{S}_n$ by a sequence of pulses at optimal times t_n to prepare a maximally entangled state in $\mathcal{S}_*$. Here, the block-diagonal structure represents the undriven Hamiltonian $\hat{H}$. (b) Illustration for a symmetric spin-1/2 chain: π pulses create $\uparrow$ spins at the center site, which then spread under the Hamiltonian, giving rise to multiple Bell pairs between mirror-conjugate sites.

a fermion at site i, yielding $\hat{H} = -(J/2)\sum_i \hat{f}_i^\dagger \hat{f}_{i+1} + \text{H.c.}$ Thus, spins $\uparrow$ and $\downarrow$ correspond to filled and empty sites, respectively, in the fermion picture. Later we will add a local interaction which will make the system nonintegrable without affecting the protocol.

Symmetry. As shown in Ref. [23], and probed experimentally in Ref. [27], there is a crucial symmetry relating to the entanglement between left and right halves of the chain, given by the symmetry operator

$$\hat{C} = \hat{\sigma}_0^z/2 + \sum_{i=1}^{l} (\hat{f}_i^\dagger \hat{f}_{-i} + \text{H.c.}). \tag{2}$$

Here, $\hat{\sigma}_0^z$ measures the fermion-number parity at the center site, and the terms $\hat{f}_i^\dagger \hat{f}_{-i}$ exchange spins between mirror-conjugate sites i and $-i$ with a phase given by the total parity in between. The nature of this exchange becomes clearer if one rewrites Eq. (2) as $\hat{C} = \hat{\sigma}_0^z/2 + \sum_{i=1}^{l}(\hat{a}_{i,+}^\dagger \hat{a}_{i,+} - \hat{a}_{i,-}^\dagger \hat{a}_{i,-})$, where $\hat{a}_{i,\pm} := (\hat{f}_i \pm \hat{f}_{-i})/\sqrt{2}$. Here, $\hat{a}_{i,\pm}^\dagger$ creates a Bell pair between sites i and $-i$, $\hat{a}_{i,\pm}^\dagger|\text{vac}\rangle \propto |{\uparrow_i}{\downarrow_{-i}}\rangle \pm |{\downarrow_i}{\uparrow_{-i}}\rangle$, where $|\text{vac}\rangle$ is the vacuum state with all spins $\downarrow$. The symmetric and antisymmetric Bell pairs can be thought of as having a "charge" of ± 1, such that $\hat{C} - \hat{\sigma}_0^z/2$ measures the net "charge" of all such pairs. Since this "charge" is 0 for the states $|{\downarrow_i}{\downarrow_{-i}}\rangle$ and $|{\uparrow_i}{\uparrow_{-i}}\rangle = \hat{a}_{i,+}^\dagger \hat{a}_{i,-}^\dagger|\text{vac}\rangle$, it *counts* the number of Bell pairs at $\{i, -i\}$ up to a sign. Therefore, the eigenvalues of $\hat{C}$ vary from $\lambda = -l - 1/2$ to $\lambda = l + 1/2$ in steps of 1, with the $\pm 1/2$ arising from $\hat{\sigma}_0^z/2$. In the extreme sectors, $\lambda = \pm(l + 1/2)$, there is a single, maximally entangled state with a Bell pair at all positions, given by $|\Psi_\pm\rangle \propto |\pm\rangle_0 \prod_{i=1}^{l}[|{\uparrow_i}{\downarrow_{-i}}\rangle + (-1)^i |{\downarrow_i}{\uparrow_{-i}}\rangle]$, where $|+\rangle \equiv |\uparrow\rangle$, $|-\rangle \equiv |\downarrow\rangle$, and the alternating phase $(-1)^i$ originates from the JW string. Smaller absolute values of λ correspond to states with fewer Bell pairs on average.

Protocol. Our strategy is to start from the vacuum state with $\lambda = -1/2$ and apply a sequence of timed pulses to reach the state $|\Psi_+\rangle$ with $\lambda = l + 1/2$. For this, one can increase λ by 1 by flipping the center spin from $\downarrow$ to $\uparrow$ [see Eq. (2)]. However, one has to ensure it does not affect the exchange terms $\hat{f}_i^\dagger \hat{f}_{-i}$ which also depend on the center spin. Thus, instead of a π pulse at the center site alone, one has to apply a fermionic pulse, e.g., $\hat{f}_0 + \hat{f}_0^\dagger \propto \hat{\sigma}_0^x \prod_{i<0} \hat{\sigma}_i^z$, which commutes with $\hat{f}_i^\dagger \hat{f}_{-i}$ $\forall i \neq 0$. This amounts to applying simultaneous local π pulses on half the qubits, which can be implemented in experiments. Under such a fermionic pulse, $\langle \hat{C} \rangle \to \langle \hat{C} \rangle - \langle \hat{\sigma}_0^z \rangle$, so if the center spin is $\downarrow$ when the pulse is applied, $\langle \hat{C} \rangle$ increases by 1.

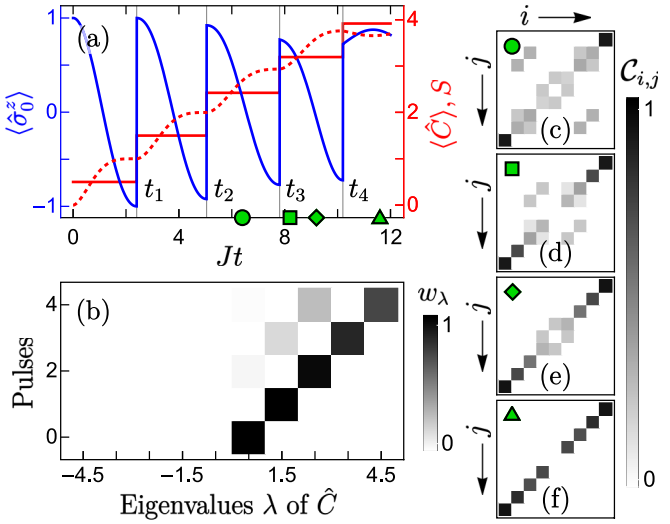

FIG. 2. (a) Time evolution of the center-spin magnetization $\langle \hat{\sigma}_0^z \rangle$ of a 9-site spin-1/2 XX chain using exact diagonalization. The center spin is flipped whenever $\langle \hat{\sigma}_0^z \rangle$ reaches a minimum below 0, which increases the expectation of the symmetry $\hat{C}$ (horizontal lines) that relates to the number of Bell pairs between mirror-conjugate sites. Accordingly, the von Neumann entropy S between two sides of the chain grows monotonically (dotted curve). (b) Weights w_λ in different symmetry sectors after each pulse, showing a high-fidelity transfer toward more strongly entangled states. (c)–(f) Pairwise concurrence $\mathcal{C}_{i,j}$ between sites i and j (with $\mathcal{C}_{i,i} \equiv 0$) at times indicated by the green labels in (a), showing how the Bell pairs at $\{i, -i\}$ are successively stacked inward until all positions are filled.

Another way to interpret the dynamics is to note that the antisymmetric modes $\hat{a}_{i,-}$ decouple and remain unoccupied throughout. Then one finds $\hat{H} = -(J/\sqrt{2})\hat{c}_0^\dagger \hat{c}_1 - (J/2)\sum_{i=1}^{l-1} \hat{c}_i^\dagger \hat{c}_{i+1} + \text{H.c.}$, where $\hat{c}_0 := \hat{f}_0$ and $\hat{c}_{i>0} := \hat{a}_{i,+}$, and the symmetry can be written as $\hat{C} = \hat{N} - 1/2$, where $\hat{N}$ is the total number of fermions. Thus, we increase $\langle \hat{C} \rangle$ by injecting fermions at site 0, until we reach $|\Psi_+\rangle$ with all the symmetric modes occupied.

Figure 1(b) shows the resulting protocol: Flipping the center spin of the vacuum state gives $\lambda = 1/2$ and produces a spin-$\uparrow$ impurity that spreads out ballistically in both directions [28], entangling those sites. During this spreading, λ is unaltered as $[\hat{H}, \hat{C}] = 0$. After a time $t_1 \sim 2/J$, the center site points $\downarrow$ again, when we apply the next pulse, producing another $\uparrow$ spin and increasing λ by 1. Repeating this process l times gets one to the state $|\Psi_+\rangle$ with l Bell pairs in a time $t_l \sim 2l/J$.

The protocol is not perfect as the center does not fully relax to a spin-$\downarrow$ state after the second pulse, as shown in Fig. 2(a). We apply the following pulses whenever $\langle \hat{\sigma}_0^z \rangle$ is minimum (and negative) for the first time. Due to the nonvanishing spin-$\uparrow$ component, there is a small likelihood that λ *decreases* by 1 during the spin flip. However, as shown in

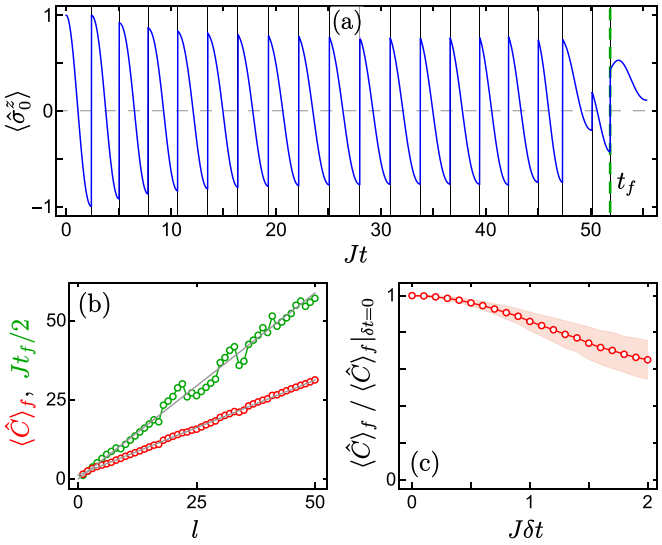

FIG. 3. (a) Evolution of the center-spin magnetization, $\langle\hat{\sigma}_0^z\rangle$, during our protocol for 47 sites ($l = 23$) using exact diagonalization. The last pulse is applied at time t_f, after which $\langle\hat{\sigma}_0^z\rangle$ reaches a minimum above 0. (b) Final value of $\langle\hat{C}\rangle$ and duration t_f as a function of l, compared with $0.6(l+2)$ and $2.35l/J$, respectively, shown by the gray lines. The sudden small fluctuations are due to variation in the number of pulses, which fluctuates around $0.8l$ for large l. (c) Relative change of $\langle\hat{C}\rangle_f$ when the timing of each pulse is randomized by $\pm\delta t$ for $l \gtrsim 10$. The dots show mean values and the shaded area shows standard deviations from 1000 trajectories.

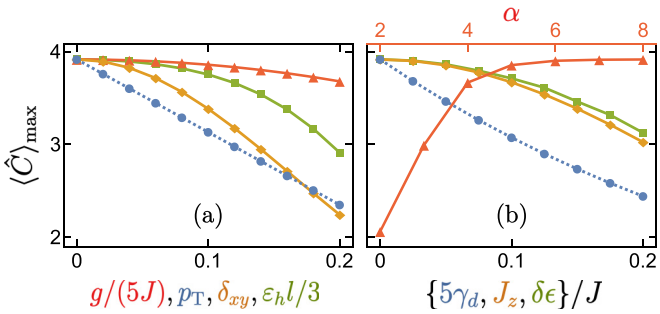

FIG. 4. Maximum value of $\langle\hat{C}\rangle$ attained for 9 sites in the presence of (a) symmetry-preserving and (b) symmetry-breaking, unitary (solid) and nonunitary (dotted) perturbations: (a) g is the strength of an integrability-breaking local coupling in $\hat{H}_g$ (see text); p_T is a defect probability of starting with an $\uparrow$ spin at any given site; δ_{xy} is the anisotropy for an XY chain, $\delta_{xy} := (J_x - J_y)/(J_x + J_y)$; ε_h is a harmonic-trap-induced inhomogeneity, such that $J_{i,i+1} = J/[1 - \varepsilon_h^2(i+1/2)^2]$ [28]; (b) γ_d is a uniform dephasing rate, modeled by Lindblad operators $\sqrt{\gamma_d}\hat{\sigma}_i^z/2$ (see Appendix E); J_z is a uniform z-z coupling; $\delta\epsilon$ is a disorder strength that gives $\delta\hat{H} = \sum_i \epsilon_i\hat{\sigma}_i^z$ where ϵ_i are randomly distributed in $[-\delta\epsilon/2, \delta\epsilon/2]$; α characterizes long-range interactions $J_{i,j} = J/|i-j|^\alpha$. For disorder, dephasing, and thermal defects, $\langle\hat{C}\rangle$ is ensemble averaged.

Fig. 2(b), the distribution remains strongly peaked at the target sector $\lambda = n + 1/2$ after the nth pulse. As a result, both $\langle\hat{C}\rangle$ and the entanglement entropy between left and right halves are near maximal at the end of the sequence [see Fig. 2(a)]. Furthermore, the entanglement is distilled in the form of Bell pairs, which is unusual even for highly entangled states [9]. Such Bell pairs between mirror-conjugate sites are seen in Fig. 2(f), where we plot the concurrence between sites i and j, computed from their reduced density matrix [29], which is a robust measure of entanglement between two qubits that increases from 0 when the qubits are not entangled to 1 when they are maximally entangled.

Figure 2(c) shows the first of these Bell pairs is established between the two end sites when the first $\uparrow$ spin arrives at $t \sim l/J$. Each subsequent pulse adds one more Bell pair toward the center [Figs. 2(d)–2(f)]. This stacking is also evident in the experimentally measurable spin-spin correlations (see Appendix B).

Finite-size scaling. The success of the protocol is characterized by the final value of $\langle\hat{C}\rangle$ which is bounded by $l + 1/2$. Figure 3(a) shows that, for large l, $\langle\hat{C}\rangle$ increases quite uniformly up to times $t \sim 2l/J$. Thereafter, $\langle\hat{\sigma}_0^z\rangle$ can reach a minimum above 0, where applying a pulse would decrease $\langle\hat{C}\rangle$, and continuing beyond this point does not lead to significant gains. Figure 3(b) shows that the resulting final value of $\langle\hat{C}\rangle$ increases linearly with l, $\langle\hat{C}\rangle_f \approx 0.6(l+2)$, i.e., the average number of Bell pairs grows linearly with the number of qubits. Furthermore, as the pulses are roughly uniformly spaced, the preparation time also scales linearly, $t_f \sim 2l/J$, as shown in Fig. 3(c). This scaling is on par with more complex protocols using two-qubit gates [6] or nonuniform coupling [14,15], and much faster than using correlated dissipation [16,23]. It could be enhanced further by optimal pulse shaping [30,31]. Moreover, one can project the final state onto $|\Psi_+\rangle$ by measuring the spin imbalance $\hat{\sigma}^z := \sum_i \hat{\sigma}_i^z$, which varies as $\hat{\sigma}^z = 2(\hat{C} - l)$ during the protocol, since λ is changed by flipping a spin. Note the Lieb-Robinson bound sets a fundamental speed limit on how fast distant parts of a locally interacting system can be entangled [32,33]. By having a preparation time that grows linearly with system size, our protocol saturates this bound.

Robustness. The protocol does not rely on the precise timing of the pulses. Figure 3(c) shows how the fidelity $\langle\hat{C}\rangle_f$ is affected if we change the timing of every intermediate pulse by a random number between $\pm\delta t$. First, $\langle\hat{C}\rangle_f$ is unaffected to linear order in δt. Second, even when $\delta t = 1/J$, which is roughly half the spacing between the ideal pulses, $\langle\hat{C}\rangle_f$ is reduced only by 15% for any size $l \gtrsim 10$.

Figure 4 shows the protocol is relatively insensitive to generic imperfections found in experiments. In particular, $\langle\hat{C}\rangle$ is affected only to second order in common Hamiltonian perturbations (see argument in Appendix D). This includes both symmetry-preserving cases, such as an x-y anisotropy, and symmetry-breaking perturbations, such as a z-z coupling, random Zeeman splittings, or next-nearest-neighbor coupling.

If a perturbation commutes with both $\hat{C}$ and $\hat{\sigma}_0^z$, the full time evolution of $\langle\hat{C}\rangle$ is unaltered, as in the case of a uniform Zeeman field $\hat{\sigma}^z$. For other symmetry-preserving perturbations, including reflection-symmetric traps [23] and dephasing at the center site, the final value of $\langle\hat{C}\rangle$ may be lower but the Bell pairs are stable. If the symmetry itself is broken, however, $\langle\hat{C}\rangle$ decreases in between pulses, attaining the maximum at an intermediate time, rather than at the end of the pulse sequence. In Fig. 4 $\langle\hat{C}\rangle_{\max}$ refers to this maximum value in symmetry-broken cases and to the final value of $\langle\hat{C}\rangle$ otherwise.

We emphasize that the protocol is of broad generality and not limited to free-fermionic models. For instance, consider the Hamiltonian $\hat{H}_g = \hat{H} - (g/4)\hat{\sigma}_0^z(\hat{\sigma}_1^z + \hat{\sigma}_{-1}^z + 1)$. Here, we have added a z-z coupling between the center spin and its neighbors and a proportional Zeeman field such that there is no energy cost for spreading an $\uparrow$ spin from site 0 to a superposition of sites 1 and -1. One can show that $\hat{H}_g$ preserves the symmetry $\hat{C}$ [23], but the z-z coupling mediates interactions between the JW fermions. In fact, $\hat{H}_g$ displays level repulsion characteristic of nonintegrability (see Appendix C). Nonetheless, Fig. 4(a) shows that the efficiency of our pulse sequence falls very slowly with g. Even for strong integrability breaking at $g = J$ we recover nearly the same finite-size scaling, with $\langle\hat{C}\rangle \approx 0.6(l+1)$ for up to $l = 25$ [Fig. 8(b)].

Experimental realization. The protocol can be implemented most naturally on experimental platforms where interacting qubits lead to the XX model in Eq. (1) and where one has the capability of single-site addressing. These include quantum-gas microscopes [34], superconducting circuits [35], and arrays of Rydberg atoms [36].

Quantum-gas microscope experiments allow one to flip the spin of individual atoms in a chain with high accuracy using a tightly focused laser beam and a microwave field [28]. Using two-component bosons at unit filling in the limit of strong interactions realizes a Heisenberg chain through virtual spin exchange [37]. By separately tuning the intra- and interspecies interactions, one can set the z-z coupling to 0, producing our spin-1/2 XX model, as in Ref. [38]. The nonintegrable Hamiltonian $\hat{H}_g$ may be engineered by tuning the local confinement for one of the spin states, which gives a residual z-z coupling between the center site and its neighbors (see Appendix C).

The nearest-neighbor XX chain has also been realized using capacitively coupled transmon qubits in a superconducting circuit [39], where signatures of the symmetry $\hat{C}$ were observed recently [27]. Here one can perform arbitrary single-qubit rotations [35]. The dominant errors come from on-site dephasing and disorder, which are both hundreds of times smaller than J in existing setups [39].

Resonant dipole-dipole interactions between Rydberg excitations in a chain of atoms also yields an XX model but with long-range coupling, $J_{i,j} = J/|i-j|^\alpha$ with $\alpha = 3$ [36], which breaks the symmetry $\hat{C}$. Nonetheless, one can obtain fidelities of up to 75% for 9 sites [Fig. 4(b)]. For trapped-ion chains [40], however, α is typically limited to smaller values, making the protocol less viable.

The pulse timings for a given setup can be determined one at a time by calibrating its evolution, e.g., by evolving the system repeatedly over a variable duration and imaging the final state, as is standard in quantum-gas microscopes [28]. One can also use first-principles numerical modeling. Furthermore, the pulses may be automated by monitoring the central spin and using conditional feedback [41,42]. However, the resulting evolution is nonunitary and we do not model it here. As Fig. 3(c) shows, the fidelity under unitary evolution remains high even if the pulse times are suboptimal.

Note that the linear dimension of the relevant experimental setups is typically limited to few tens of sites and one can probe the dynamics for at least several tens of tunneling time [27,28,38,39]. Our findings are accessible in this regime [see Fig. 3(b)].

Generalizations: η pairing. Having demonstrated our approach for a spin chain, we now consider the celebrated Fermi-Hubbard model [25] with $2l$ sites,

$$\hat{H}_F = \sum_{s=\uparrow,\downarrow}\sum_{i=1}^{2l-1}(-J\hat{c}_{i,s}^\dagger\hat{c}_{i+1,s} + \text{H.c.}) + U\sum_{i=1}^{2l}\hat{n}_{i,\uparrow}\hat{n}_{i,\downarrow}\,. \quad (3)$$

Here, $\hat{c}_{i,s}^\dagger$ creates a fermion with spin s at site i, $\hat{n}_{i,s} := \hat{c}_{i,s}^\dagger\hat{c}_{i,s}$ gives the site occupation, J is now the nearest-neighbor tunneling, and $U > 0$ is an on-site repulsion. It has been known since the 1990s that $\hat{H}$ has eigenstates with long-range superconducting order [26], thanks to an SU(2) symmetry with generators $\hat{\eta}^- = \sum_i(-1)^i\hat{c}_{i,\uparrow}\hat{c}_{i,\downarrow}$, $\hat{\eta}^+ = \hat{\eta}^{-\dagger}$, and $\hat{\eta}^z = \sum_i(\hat{n}_{i,\uparrow} + \hat{n}_{i,\downarrow} - 1)/2$. Here, $\hat{\eta}^+$ acting on the vacuum $|0\rangle$ creates a bound pair (doublon) with quasimomentum π (an η pair), which leads to staggered superconducting pair correlations $P_{i,j} = \langle\hat{c}_{i,\downarrow}^\dagger\hat{c}_{i,\uparrow}^\dagger\hat{c}_{j,\uparrow}\hat{c}_{j,\downarrow}\rangle$. In particular, at half filling ($\hat{\eta}_z = 0$), the correlations are maximal for an η condensate $|Y\rangle \propto (\hat{\eta}^+)^l|0\rangle$, which gives $P_{i,j} = (-1)^{i+j}l/(4l-2)\ \forall i \neq j$ [26]. However, producing an η pair costs energy U, so $|Y\rangle$ is a highly excited state that is difficult to engineer in theory [43–50] and has not been realized experimentally.

To prepare $|Y\rangle$ using pulses, we note that the number of η pairs, N_η, is measured by the symmetry $\hat{\eta}^2 = \hat{\eta}^+\hat{\eta}^- - \hat{\eta}^z + (\hat{\eta}^z)^2$ with eigenvalues $N_\eta(N_\eta+1)$, where $N_\eta = 0, 1, \ldots, l$ at half filling. The maximally correlated $|Y\rangle$ is the only state having $N_\eta = l$. Further, as shown in Ref. [44], one can change N_η by ± 1 by applying the current operator $\hat{\mathcal{J}} = \mathrm{i}\sum_{i,s}\hat{c}_{i+1,s}^\dagger\hat{c}_{i,s} + \text{H.c.}$: This amounts to changing $J \to \mathrm{i}J'(t)$ in Eq. (3) for a short pulse, which would be challenging to implement for neutral atoms, but possible via laser-assisted tunneling [51] or lattice shaking [52].

Thus, we arrive at a conceptually simple protocol: Starting from an antiferromagnetic ground state with $N_\eta = 0$ for $U \gg J$, as realized in Ref. [53], we repeatedly apply $\hat{\mathcal{J}}$ when it would increase $\langle\hat{\eta}^2\rangle$ the most. To this end, we monitor $\mathcal{T} := \langle\hat{\mathcal{J}}\hat{\eta}^2\hat{\mathcal{J}}\rangle/\langle\hat{\mathcal{J}}^2\rangle$ and apply the next pulse whenever $\mathcal{T}$ is maximum over a virtual-tunneling time $\Delta t = U/(2J^2)$, the slowest timescale in the problem, as illustrated in Fig. 5. Figure 6(a) shows that the state after l pulses has a significant overlap with $|Y\rangle$, which is reached in a time $t \sim 6/J$ for 8 sites, which is much faster than adiabatic [43] or dissipative [50] approaches for the same system size. The η pairing is manifest in the pair-momentum distribution $N(q) = (2l)^{-1}\sum_{i,j}e^{\mathrm{i}q(i-j)}P_{i,j}$ as a sharp peak at $q = \pi$ [Fig. 6(b)], which can be detected experimentally [54]. Note that the final value of $\langle\hat{\eta}^2\rangle$ grows linearly with l [Fig. 6(c)], so the average number of η pairs grows as $\sqrt{l}$. The preparation time is bounded by $l\Delta t$.

The Hubbard model also has a spin-SU(2) symmetry whose generators $\hat{S}^\pm$ and $\hat{S}^z$ are related to the η generators by a particle-hole transformation $c_{i,\downarrow} \to (-1)^i\hat{c}_{i,\downarrow}^\dagger$ [25]. Hence, there is a dual protocol for maximizing the total spin $\langle\hat{S}^2\rangle$ for long-range spin-spin correlations, with the pulse operator $\hat{\mathcal{J}}_s = \mathrm{i}\sum_i\hat{c}_{i+1,\uparrow}^\dagger\hat{c}_{i,\uparrow} - \hat{c}_{i+1,\downarrow}^\dagger\hat{c}_{i,\downarrow} + \text{H.c.}$, i.e., a spin-dependent complex tunneling as in Ref. [55].

Note that our approach is distinct from other nonadiabatic protocols for η pairing in the literature, which we briefly summarize. References [45,46] employ quasilocal dissipative drives, modeled by an extensive number of quartic and higher-order two-site Lindblad operators, that drive the system to $|Y\rangle$.

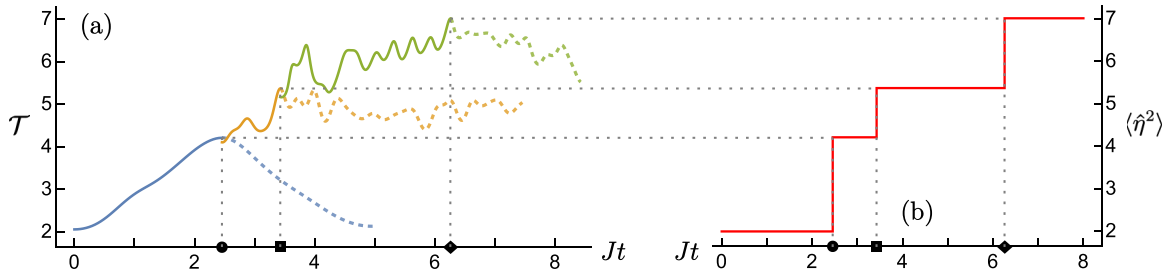

FIG. 5. Generation of η pairs in a Fermi-Hubbard chain with 8 sites and $U/J = 10$, starting from an antiferromagnetic ground state at half filling, from exact diagonalization. (a) Efficacy $\mathcal{T} := \langle\hat{\mathcal{J}}\hat{\eta}^2\hat{\mathcal{J}}\rangle/\langle\hat{\mathcal{J}}^2\rangle$ is monitored for a duration $U/(2J^2)$ and the next pulse of $\hat{\mathcal{J}}$ is applied when $\mathcal{T}$ is maximum, shown by the dotted vertical lines. Solid curves show the resulting piecewise evolution. (b) $\langle\hat{\eta}^2\rangle$ is conserved in between pulses and jumps to the instantaneous value of $\mathcal{T}$ after the application of each pulse (black dots).

However, engineering such dissipators is nontrivial and has not been realized. References [47–49] use heating within a symmetry sector to distribute correlations already present in the initial state over all distances. Crucially, there is no mechanism to switch sectors, and starting from the ground state yields $\langle\hat{\eta}^2\rangle \propto 1/l$. Reference [44] is closer to our approach in that they use a unitary drive that breaks the SU(2) symmetry. However, they apply a single extended pulse and produce no overlap with $|Y\rangle$ for any system size.

Conclusions. We have introduced a technique that uses global symmetries to produce on-demand long-range entanglement and strong quantum correlations. The approach relies on the symmetry structure and can be extended to dissipative systems [23,47,49] and higher dimensions [26,56]. For simplicity, we have used optimally timed instantaneous pulses; one should be able to obtain even higher fidelities by allowing more general waveforms with optimal control strategies [30,31,44]. Furthermore, it may be possible to automate the pulse timings with continuous monitoring and feedback [41,42]: The knowledge gained from measurements can further help steer the system to the desired state, which would be useful to explore in future studies. Together with advances in engineering many-body Hamiltonians [34–36,40,57] and dissipation [58,59], our technique paves an exciting route to synthesizing strongly-entangled quantum states with key applications to quantum information processing.

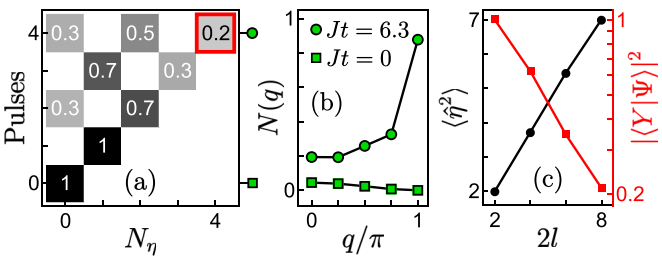

FIG. 6. Results for the η-pairing protocol with strong repulsive interactions ($U/J = 10$). (a) Distribution among symmetry sectors of $\hat{\eta}^2$ with different numbers of η pairs, N_η, after successive pulses for $2l = 8$ sites. The red square highlights a notable overlap with the maximally correlated η condensate $|Y\rangle$. (b) Initial and final pair-momentum distributions, showing the emergence of a peak at the band edge, characteristic of η pairing. (c) The final value of $\langle\hat{\eta}^2\rangle$ grows linearly with l, but the many-body overlap with $|Y\rangle$ falls exponentially [43].

Data supporting this publication are available in the Apollo repository [60].

Acknowledgments. We thank Leonardo Banchi, Berislav Buča, and Klaus Mølmer for useful discussions. This work was supported by EPSRC Grant No. EP/P009565/1 and by a Simons Investigator Award, Grant No. 511029.

Appendix A: Equation of motion for the qubit array. Our protocol for generating Bell pairs leads to a closed evolution of the two-point correlations $\langle\hat{f}_i^\dagger\hat{f}_j\rangle$ and $\langle\hat{f}_i\hat{f}_j\rangle$, where $\hat{f}_i$ are the Jordan-Wigner (JW) fermions. In between pulses, they evolve under the free-fermion Hamiltonian, which gives

$$\partial_t\langle\hat{f}_i^\dagger\hat{f}_j\rangle = \frac{iJ}{2}\langle\hat{f}_i^\dagger\hat{f}_{j+1} + \hat{f}_i^\dagger\hat{f}_{j-1} - \hat{f}_{i+1}^\dagger\hat{f}_j - \hat{f}_{i-1}^\dagger\hat{f}_j\rangle, \quad \text{(A1a)}$$

$$\partial_t\langle\hat{f}_i\hat{f}_j\rangle = \frac{iJ}{2}\langle\hat{f}_i\hat{f}_{j+1} + \hat{f}_i\hat{f}_{j-1} + \hat{f}_{i+1}\hat{f}_j + \hat{f}_{i-1}\hat{f}_j\rangle \quad \text{(A1b)}$$

$\forall i, j$, with $\hat{f}_{l+1} := \hat{f}_{-l-1} := 0$. A fermionic pulse $\hat{f}_0 + \hat{f}_0^\dagger$ changes the expectation $\langle\hat{O}\rangle$ to $\langle(\hat{f}_0^\dagger + \hat{f}_0)\hat{O}(\hat{f}_0 + \hat{f}_0^\dagger)\rangle$, which couples $\langle\hat{f}_i^\dagger\hat{f}_j\rangle$ and $\langle\hat{f}_i\hat{f}_j\rangle$ through the substitutions

$$\langle\hat{f}_0^\dagger\hat{f}_0\rangle \longrightarrow 1 - \langle\hat{f}_0^\dagger\hat{f}_0\rangle, \quad \text{(A2a)}$$

$$\langle\hat{f}_i^\dagger\hat{f}_0\rangle \longleftrightarrow \langle\hat{f}_i\hat{f}_0\rangle^* \quad \forall i \neq 0, \quad \text{(A2b)}$$

$$\langle\hat{f}_0^\dagger\hat{f}_i\rangle \longleftrightarrow -\langle\hat{f}_0\hat{f}_i\rangle \quad \forall i \neq 0. \quad \text{(A2c)}$$

Such a pulse is applied when $\langle\hat{\sigma}_0^z\rangle$ reaches a minimum below 0. Using $\hat{\sigma}_0^z = 2\hat{f}_0^\dagger\hat{f}_0 - 1$ and Eq. (A1a) yields

$$\partial_t\langle\hat{\sigma}_0^z\rangle = 2J\,\mathrm{Im}\langle\hat{f}_{-1}^\dagger\hat{f}_0 - \hat{f}_0^\dagger\hat{f}_1\rangle, \quad \text{(A3a)}$$

$$\partial_t^2\langle\hat{\sigma}_0^z\rangle = J^2\,\mathrm{Re}\langle\hat{f}_{-1}^\dagger\hat{f}_{-1} + \hat{f}_1^\dagger\hat{f}_1 - 2\hat{f}_0^\dagger\hat{f}_0 + 2\hat{f}_{-1}^\dagger\hat{f}_1 - \hat{f}_{-2}^\dagger\hat{f}_0 - \hat{f}_0^\dagger\hat{f}_2\rangle, \quad \text{(A3b)}$$

where Re and Im denote real and imaginary parts. Thus, starting with a single ↑ spin at $i = 0$, we evolve Eqs. (A1a) and (A1b), making the changes in Eqs. (A2a)–(A2c) whenever $\partial_t\langle\hat{\sigma}_0^z\rangle = 0$, $\partial_t^2\langle\hat{\sigma}_0^z\rangle > 0$, and $\langle\hat{\sigma}_0^z\rangle < 0$, for up to l times, as shown in Figs. 2(a) and 3(a).

Appendix B: Spin-spin correlations. The Bell pairs can be detected in experiments by measuring the spin-spin correlations $\langle\hat{\sigma}_i^\nu\hat{\sigma}_j^\nu\rangle$ for $\nu = x, y, z$, plotted in Fig. 7. Since the dynamics are generated by a quadratic Hamiltonian, the many-body state is Gaussian [61] and we can find $\langle\hat{\sigma}_i^\nu\hat{\sigma}_j^\nu\rangle$ from $\langle\hat{f}_i^\dagger\hat{f}_j\rangle$ and $\langle\hat{f}_i\hat{f}_j\rangle$ using Wick's theorem. To this end,

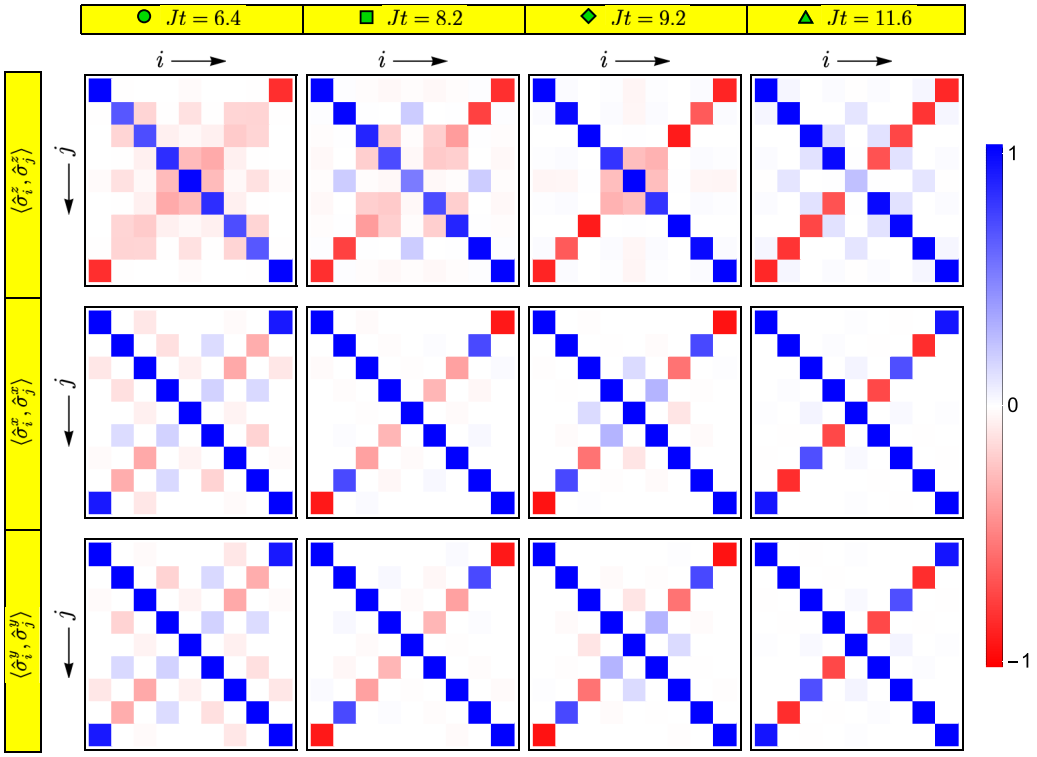

FIG. 7. Spin-spin correlations $\langle \hat{\sigma}_i^{\nu}, \hat{\sigma}_j^{\nu} \rangle := \langle \hat{\sigma}_i^{\nu} \hat{\sigma}_j^{\nu} \rangle - \langle \hat{\sigma}_i^{\nu} \rangle \langle \hat{\sigma}_j^{\nu} \rangle$ for a 9-site XX chain from exact diagonalization, corresponding to Figs. 2(c)–2(f) in the main text, reflecting the successive stacking of Bell pairs between mirror-conjugate sites. Pulses are applied at times $Jt = 2.4, 5.0, 7.8, 10.2$, whereby the phase correlations $\langle \hat{\sigma}_i^{x}, \hat{\sigma}_{-i}^{x} \rangle$ and $\langle \hat{\sigma}_i^{y}, \hat{\sigma}_{-i}^{y} \rangle$ flip sign. Note that $\langle \hat{\sigma}_i^{x} \rangle = \langle \hat{\sigma}_i^{y} \rangle = 0 \; \forall t$.

we first define $\hat{A}_i := \hat{f}_i^{\dagger} + \hat{f}_i$ and $\hat{B}_i := \hat{f}_i^{\dagger} - \hat{f}_i$. Substituting $\hat{\sigma}_i^z = \hat{B}_i \hat{A}_i$ in the JW transformation gives, for $i < j$,

$$\langle \hat{\sigma}_i^z \hat{\sigma}_j^z \rangle = \langle \hat{B}_i \hat{A}_i \hat{B}_j \hat{A}_j \rangle \,, \tag{B1a}$$

$$\langle \hat{\sigma}_i^x \hat{\sigma}_j^x \rangle = \left\langle \prod_{k=i}^{j-1} \hat{B}_k \hat{A}_{k+1} \right\rangle, \tag{B1b}$$

$$\langle \hat{\sigma}_i^y \hat{\sigma}_j^y \rangle = (-1)^{j-i} \left\langle \prod_{k=i}^{j-1} \hat{A}_k \hat{B}_{k+1} \right\rangle. \tag{B1c}$$

Applying Wick's theorem to Eq. (B1a), we find

$$\langle \hat{\sigma}_i^z \hat{\sigma}_j^z \rangle = \langle \hat{B}_i \hat{A}_i \rangle \langle \hat{B}_j \hat{A}_j \rangle - \langle \hat{B}_i \hat{B}_j \rangle \langle \hat{A}_i \hat{A}_j \rangle + \langle \hat{B}_i \hat{A}_j \rangle \langle \hat{A}_i \hat{B}_j \rangle \,. \tag{B2}$$

Similarly, the string correlation in $\langle \hat{\sigma}_i^x \hat{\sigma}_j^x \rangle$ [Eq. (B1b)] can be reduced to the Pfaffian of an antisymmetric matrix $\mathbf{\Gamma}^x$ [62] of size $2(j-i)$, with the elements

$$\Gamma^x_{m,n} = \begin{pmatrix} \langle \hat{B}_m \hat{B}_n \rangle + \delta_{m,n} & \langle \hat{B}_m \hat{A}_{n+1} \rangle \\ \langle \hat{A}_{m+1} \hat{B}_n \rangle & \langle \hat{A}_{m+1} \hat{A}_{n+1} \rangle - \delta_{m,n} \end{pmatrix}, \tag{B3}$$

where $m, n = i, i+1, \ldots, j-1$. One can find $\Gamma^x_{m,n}$ using

$$\langle \hat{A}_m \hat{A}_n \rangle = \delta_{m,n} + 2\mathrm{i}\,\mathrm{Im}\left\langle \hat{f}_m \hat{f}_n + \hat{f}_m^{\dagger} \hat{f}_n \right\rangle, \tag{B4a}$$

$$\langle \hat{B}_m \hat{B}_n \rangle = -\delta_{m,n} + 2\mathrm{i}\,\mathrm{Im}\left\langle \hat{f}_m \hat{f}_n - \hat{f}_m^{\dagger} \hat{f}_n \right\rangle, \tag{B4b}$$

$$\langle \hat{A}_m \hat{B}_n \rangle = \delta_{m,n} - 2\mathrm{i}\,\mathrm{Re}\left\langle \hat{f}_m \hat{f}_n + \hat{f}_m^{\dagger} \hat{f}_n \right\rangle, \tag{B4c}$$

$$\langle \hat{B}_m \hat{A}_n \rangle = -\langle \hat{A}_n \hat{B}_m \rangle \,. \tag{B4d}$$

From Eq. (B1c), $\langle \hat{\sigma}_i^y \hat{\sigma}_j^y \rangle$ is obtained by interchanging $\hat{A}$ and $\hat{B}$ in $\mathbf{\Gamma}^x$ and multiplying its Pfaffian by $(-1)^{j-i}$.

Appendix C: Integrability breaking. As discussed in the main text, our protocol also works well in the presence of a central z-z coupling described by the full Hamiltonian $\hat{H}_g = \hat{H} - (g/4)\hat{\sigma}_0^z(\hat{\sigma}_1^z + \hat{\sigma}_{-1}^z + 1)$. This coupling translates to a density-density interaction between the JW fermions at sites 0 and ± 1, so the model is no longer free fermionic. By setting the occupations of the antisymmetric modes, $\hat{f}_i - \hat{f}_{-i}$, to zero we find a reduced many-body Hamiltonian governing the dynamics in between pulses,

$$\hat{H}_g = -\frac{J}{\sqrt{2}} \hat{c}_0^{\dagger} \hat{c}_1 - \frac{J}{2} \sum_{i=1}^{l-1} (\hat{c}_i^{\dagger} \hat{c}_{i+1} + \mathrm{H.c.}) - \frac{g}{4} (-1)^{\hat{c}_0^{\dagger}\hat{c}_0 + \hat{c}_1^{\dagger}\hat{c}_1}, \tag{C1}$$

where $\hat{c}_0 := \hat{f}_0$ and $\hat{c}_{i>0} := (\hat{f}_i + \hat{f}_{-i})/\sqrt{2}$. Clearly, $\hat{H}_g$ conserves the total fermion number $\hat{N} = \sum_{i=0}^{l} \hat{c}_i^{\dagger} \hat{c}_i$, which is related to the symmetry $\hat{C}$ as $\hat{C} = \hat{N} - 1/2$.

Within each fermion-number sector, the energy spectrum exhibits level repulsion characteristic of nonintegrability. In particular, we study the distribution $P(r)$ of the ratio of consecutive level spacings, $r := (E_{n+1} - E_n)/(E_n - E_{n-1})$, proposed in Ref. [64]. Prior studies have shown that for an integrable system the level spacings are Poisson distributed, which gives $P(r) \propto 1/(1+r)^2$, whereas for a nonintegrable system the spacings follow Wigner-Dyson statistics of a

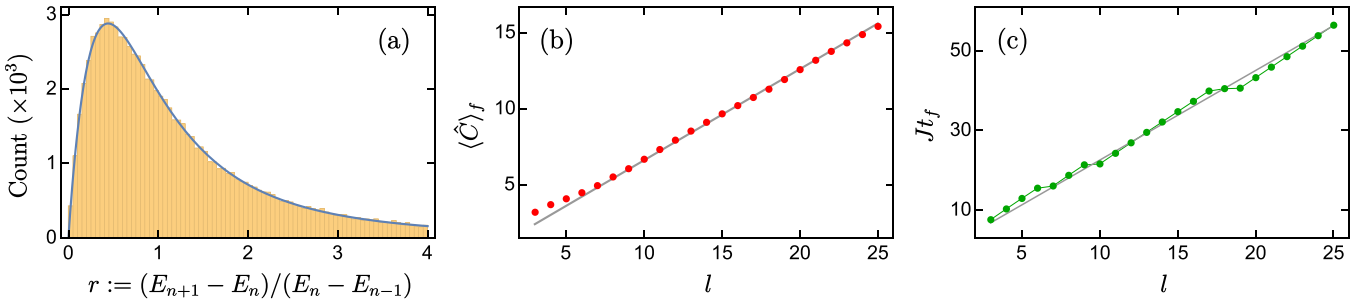

FIG. 8. (a) Distribution of the ratio of consecutive energy gaps for the model in Eq. (C1) with $g/J = 1$ and $l = 18$ in the sectors $N = 9, 10$, showing level repulsion. The solid line is a fit by a Wigner-like surmise with Dyson index $\beta \approx 0.93$ [63]. (b) Final value of $\langle \hat{C} \rangle$ and (c) preparation time as a function of l for our protocol; gray lines show $0.6(l + 1)$ and $2.25l$, respectively.

random-matrix ensemble, yielding $P(r) \propto (r + r^2)^\beta/(1 + r + r^2)^{1+(3/2)\beta}$ for a Dyson index β [63]. For $g \neq 0$ we find the latter distribution, as shown in Fig. 8(a) for the largest sector with $g = J$. This strongly suggests that the system is not only interacting but also nonintegrable.

Nonetheless, Figs. 8(b) and 8(c) show that the finite-size scaling is almost unaltered from the noninteracting case ($g = 0$) for the same pulse protocol as in Fig. 3.

To realize this model in experiments, one can use ultracold bosons with spin states $\sigma = \uparrow, \downarrow$ in a deep optical lattice. As detailed in Refs. [37,65], for unit filling their dynamics map onto an anisotropic Heisenberg chain where the spin exchange results from virtual hopping. The XX chain is realized by setting the on-site interactions $U_i^{\uparrow\uparrow} = U_i^{\downarrow\downarrow} = 2U_i^{\uparrow\downarrow}$ for all sites i [38]. To retain a z-z coupling between site 0 and ± 1, one can change the local confinement for spin $\uparrow$ at site 0, which would alter its Wannier function and the local interaction strengths. Then the central z-z coupling is given by

$$g = \frac{t_\uparrow^2 + t_\downarrow^2}{U_0^{\uparrow\downarrow}} - \frac{2t_\uparrow^2}{U_0^{\uparrow\uparrow}} - \frac{2t_\downarrow^2}{U_0^{\downarrow\downarrow}}, \tag{C2}$$

where t_σ is the hopping amplitude for spin σ.

Appendix D: First-order correction for hamiltonian perturbations. In the presence of a perturbation $\epsilon \hat{H}'$, the dynamics are generated by $\hat{U}(t) = e^{-i(\hat{H} + \epsilon \hat{H}')t}$ (with $\hbar = 1$). Using a dual of the Baker-Campbell-Hausdorff formula (called the Zassenhaus formula [66]), we write

$$\hat{U}^\dagger(t) = e^{i\hat{H}t}[1 - \epsilon \hat{P}(t) + \mathcal{O}(\epsilon^2)], \tag{D1}$$

where $\hat{P}(t)$ is an anti-Hermitian operator given by

$$\hat{P}(t) = \sum_{n=1}^{\infty} \frac{(-it)^n}{n!} [(\hat{H})^{n-1}, \hat{H}'], \tag{D2}$$

$$\text{with } [(\hat{H})^n, \hat{H}'] := \Big[\underbrace{\hat{H}, \ldots [\hat{H}, [\hat{H}}_{n \text{ times}}, \hat{H}']] \ldots \Big], \tag{D3}$$

and $[(\hat{H})^0, \hat{H}'] := \hat{H}'$. Hence, the change in the expectation value of an operator $\hat{O}$ at time t is

$$\begin{aligned} \delta\langle \hat{O} \rangle(t) &= \langle \Psi(0)| \hat{U}^\dagger(t)\, \hat{O}\, \hat{U}(t) - e^{i\hat{H}t}\, \hat{O}\, e^{-i\hat{H}t} |\Psi(0)\rangle \\ &= \epsilon \langle \Psi(t)| [\hat{O}, \hat{P}(t)] |\Psi(t)\rangle + \mathcal{O}(\epsilon^2), \end{aligned} \tag{D4}$$

where $|\Psi(t)\rangle$ is the unperturbed state. So, the first-order correction vanishes provided $\langle [\hat{O}, \hat{P}(t)] \rangle = 0$. From Eq. (D2), this is true at all times if $\langle [\hat{O}, [(\hat{H})^n, \hat{H}']] \rangle = 0 \; \forall n$. This condition is, in fact, satisfied for the operators $\hat{C}$ and $\hat{\sigma}_0^z$ for a number of common perturbations $\hat{H}'$, leading to the quadratic variations in Fig. 4.

Appendix E: Equation of motion with perturbations. The dynamics of the qubit array remain free fermionic for a number of variations, including nonuniform coupling J_i, Zeeman splittings ϵ_i, and dephasing rates $\gamma_i > 0$. The first two are described by the Hamiltonian

$$\hat{H} = -\frac{1}{2} \sum_{i=-l}^{l-1} \left(J_i \hat{f}_i^\dagger \hat{f}_{i+1} + \text{H.c.} \right) + \sum_{i=-l}^{l} \epsilon_i \hat{f}_i^\dagger \hat{f}_i, \tag{E1}$$

whereas the dephasing can be modeled by Lindblad operators $\hat{L}_i = \sqrt{\gamma_i}\, \hat{\sigma}_i^z/2$ under a standard Born-Markov approximation [67], resulting in the evolution

$$\partial_t \langle \hat{O} \rangle = i\langle [\hat{H}, \hat{O}] \rangle + \sum_i \left\langle \left[\hat{L}_i, [\hat{O}, \hat{L}_i] \right] \right\rangle \tag{E2}$$

for any Hermitian operator $\hat{O}$. The dephasing causes local coherences to decay at a rate γ_i, i.e., $\partial_t \langle \hat{\sigma}_i^x \rangle_L = -\gamma_i \langle \hat{\sigma}_i^x \rangle$, where the subscript L denotes the dephasing component. The correlations $\langle \hat{f}_i^\dagger \hat{f}_j \rangle$ and $\langle \hat{f}_i \hat{f}_j \rangle$ again form a closed set of equations, which can be found from Eq. (E2) by straightforward algebra.

Similarly, one can include an XY anisotropy $\delta_{xy} = (J_x - J_y)/(J_x + J_y)$, which adds pairing terms $\hat{f}_i \hat{f}_j$ to the Hamiltonian. For other perturbations such as a z-z coupling, long-range interactions, or incoherent spin flips in the bulk, the system is no longer free fermionic and we perform a many-body simulation.

[1] R. Horodecki, P. Horodecki, M. Horodecki, and K. Horodecki, Quantum entanglement, Rev. Mod. Phys. **81**, 865 (2009).

[2] S. Wehner, D. Elkouss, and R. Hanson, Quantum internet: A vision for the road ahead, Science **362**, eaam9288 (2018).

[3] J. Hofmann, M. Krug, N. Ortegel, L. Gérard, M. Weber, W. Rosenfeld, and H. Weinfurter, Heralded entanglement between widely separated atoms, Science **337**, 72 (2012).

[4] P. Kurpiers *et al.*, Deterministic quantum state transfer and remote entanglement using microwave photons, Nature (London) **558**, 264 (2018).

[5] P. C. Humphreys, N. Kalb, J. P. J. Morits, R. N. Schouten, R. F. L. Vermeulen, D. J. Twitchen, M. Markham, and R. Hanson, Deterministic delivery of remote entanglement on a quantum network, Nature (London) **558**, 268 (2018).

[6] P. Barmettler, A. M. Rey, E. Demler, M. D. Lukin, I. Bloch, and V. Gritsev, Quantum many-body dynamics of coupled double-well superlattices, Phys. Rev. A **78**, 012330 (2008).

[7] G. J. Mooney, G. A. L. White, C. D. Hill, and L. C. L. Hollenberg, Whole-device entanglement in a 65-qubit superconducting quantum computer, Adv. Quantum Technol. **4**, 2100061 (2021).

[8] D. Bluvstein *et al.*, A quantum processor based on coherent transport of entangled atom arrays, Nature (London) **604**, 451 (2022).

[9] V. Kendon, K. Nemoto, and W. Munro, Typical entanglement in multiple-qubit systems, J. Mod. Opt. **49**, 1709 (2002).

[10] X. Wang, A. Bayat, S. G. Schirmer, and S. Bose, Robust entanglement in antiferromagnetic Heisenberg chains by single-spin optimal control, Phys. Rev. A **81**, 032312 (2010).

[11] I. Sainz, G. Burlak, and A. B. Klimov, Entanglement generation in a spin chain by a pulsed magnetic field: analytical treatment, Eur. Phys. J. D **65**, 627 (2011).

[12] A. Bayat, S. Bose, and P. Sodano, Entanglement routers using macroscopic singlets, Phys. Rev. Lett. **105**, 187204 (2010).

[13] M. P. Estarellas, I. D'Amico, and T. P. Spiller, Robust quantum entanglement generation and generation-plus-storage protocols with spin chains, Phys. Rev. A **95**, 042335 (2017).

[14] C. Di Franco, M. Paternostro, and M. S. Kim, Nested entangled states for distributed quantum channels, Phys. Rev. A **77**, 020303(R) (2008).

[15] B. Alkurtass, L. Banchi, and S. Bose, Optimal quench for distance-independent entanglement and maximal block entropy, Phys. Rev. A **90**, 042304 (2014).

[16] A. Pocklington, Y.-X. Wang, Y. Yanay, and A. A. Clerk, Stabilizing volume-law entangled states of fermions and qubits using local dissipation, Phys. Rev. B **105**, L140301 (2022).

[17] I. Pitsios *et al.*, Photonic simulation of entanglement growth and engineering after a spin chain quench, Nat. Commun. **8**, 1569 (2017).

[18] G. Vitagliano, A. Riera, and J. I. Latorre, Volume-law scaling for the entanglement entropy in spin-1/2 chains, New J. Phys. **12**, 113049 (2010).

[19] G. Ramírez, J. Rodríguez-Laguna, and G. Sierra, From conformal to volume law for the entanglement entropy in exponentially deformed critical spin 1/2 chains, J. Stat. Mech. (2014) P10004.

[20] H. J. Briegel and R. Raussendorf, Persistent entanglement in arrays of interacting particles, Phys. Rev. Lett. **86**, 910 (2001).

[21] C. M. Langlett, Z.-C. Yang, J. Wildeboer, A. V. Gorshkov, T. Iadecola, and S. Xu, Rainbow scars: From area to volume law, Phys. Rev. B **105**, L060301 (2022).

[22] A. I. Lotkov, V. Gritsev, A. K. Fedorov, and D. V. Kurlov, Floquet integrability and long-range entanglement generation in the one-dimensional quantum Potts model, Phys. Rev. B **105**, 144306 (2022).

[23] S. Dutta and N. R. Cooper, Long-range coherence and multiple steady states in a lossy qubit array, Phys. Rev. Lett. **125**, 240404 (2020).

[24] S.-L. Ma, J. Zhang, X.-K. Li, Y.-L. Ren, J.-K. Xie, M.-T. Cao, and F.-L. Li, Coupling-modulation–mediated generation of stable entanglement of superconducting qubits via dissipation, Europhys. Lett. **135**, 63001 (2021).

[25] F. H. L. Essler, H. Frahm, F. Göhmann, A. Klümper, and V. E. Korepin, *The One-Dimensional Hubbard Model* (Cambridge University Press, Cambridge, UK, 2005).

[26] C. N. Yang, η pairing and off-diagonal long-range order in a Hubbard model, Phys. Rev. Lett. **63**, 2144 (1989).

[27] L. Li *et al.*, Observation of multiple steady states with engineered dissipation, arXiv:2308.13235.

[28] T. Fukuhara *et al.*, Quantum dynamics of a mobile spin impurity, Nat. Phys. **9**, 235 (2013).

[29] W. K. Wootters, Entanglement of formation of an arbitrary state of two qubits, Phys. Rev. Lett. **80**, 2245 (1998).

[30] N. Khaneja, T. Reiss, C. Kehlet, T. Schulte-Herbrüggen, and S. J. Glaser, Optimal control of coupled spin dynamics: design of NMR pulse sequences by gradient ascent algorithms, J. Magn. Res. **172**, 296 (2005).

[31] J.-S. Li, J. Ruths, T.-Y. Yu, H. Arthanari, and G. Wagner, Optimal pulse design in quantum control: A unified computational method, Proc. Natl. Acad. Sci. USA **108**, 1879 (2011).

[32] S. Bravyi, M. B. Hastings, and F. Verstraete, Lieb-Robinson bounds and the generation of correlations and topological quantum order, Phys. Rev. Lett. **97**, 050401 (2006).

[33] C.-F. Chen, A. Lucas, and Y. Chao, Speed limits and locality in many-body quantum dynamics, Rep. Prog. Phys. **86**, 116001 (2023).

[34] C. Gross and I. Bloch, Quantum simulations with ultracold atoms in optical lattices, Science **357**, 995 (2017).

[35] A. Blais, A. L. Grimsmo, S. M. Girvin, and A. Wallraff, Circuit quantum electrodynamics, Rev. Mod. Phys. **93**, 025005 (2021).

[36] A. Browaeys and T. Lahaye, Many-body physics with individually controlled Rydberg atoms, Nat. Phys. **16**, 132 (2020).

[37] L.-M. Duan, E. Demler, and M. D. Lukin, Controlling spin exchange interactions of ultracold atoms in optical lattices, Phys. Rev. Lett. **91**, 090402 (2003).

[38] P. N. Jepsen, J. Amato-Grill, I. Dimitrova, W. W. Ho, E. Demler, and W. Ketterle, Spin transport in a tunable Heisenberg model realized with ultracold atoms, Nature (London) **588**, 403 (2020).

[39] R. Ma, B. Saxberg, C. Owens, N. Leung, Y. Lu, J. Simon, and D. I. Schuster, A dissipatively stabilized Mott insulator of photons, Nature (London) **566**, 51 (2019).

[40] C. Monroe *et al.*, Programmable quantum simulations of spin systems with trapped ions, Rev. Mod. Phys. **93**, 025001 (2021).

[41] H. M. Wiseman and G. J. Milburn, *Quantum Measurement and Control* (Cambridge University Press, Cambridge, UK, 2009).

[42] S. Hacohen-Gourgy and L. S. Martin, Continuous measurements for control of superconducting quantum circuits, Adv. Phys. X **5**, 1813626 (2020).

[43] A. Kantian, A. J. Daley, and P. Zoller, η condensate of fermionic atom pairs via adiabatic state preparation, Phys. Rev. Lett. **104**, 240406 (2010).

[44] T. Kaneko, T. Shirakawa, S. Sorella, and S. Yunoki, Photoinduced η pairing in the Hubbard model, Phys. Rev. Lett. **122**, 077002 (2019).

[45] S. Diehl, A. Micheli, A. Kantian, B. Kraus, H. P. Büchler, and P. Zoller, Quantum states and phases in driven open quantum systems with cold atoms, Nat. Phys. **4**, 878 (2008).

[46] B. Kraus, H. P. Büchler, S. Diehl, A. Kantian, A. Micheli, and P. Zoller, Preparation of entangled states by quantum Markov processes, Phys. Rev. A **78**, 042307 (2008).

[47] J. Tindall, B. Buča, J. R. Coulthard, and D. Jaksch, Heating-induced long-range η pairing in the Hubbard model, Phys. Rev. Lett. **123**, 030603 (2019).

[48] J. Tindall, F. Schlawin, M. A. Sentef, and D. Jaksch, Analytical solution for the steady states of the driven Hubbard model, Phys. Rev. B **103**, 035146 (2021).

[49] M. Nakagawa, N. Tsuji, N. Kawakami, and M. Ueda, η pairing of light-emitting fermions: Nonequilibrium pairing mechanism at high temperatures, arXiv:2103.13624.

[50] X. Z. Zhang and Z. Song, Dynamical preparation of a steady off-diagonal long-range order state in the Hubbard model with a local non-Hermitian impurity, Phys. Rev. B **102**, 174303 (2020).

[51] N. Goldman, G. Juzeliūnas, P. Öhberg, and I. B. Spielman, Light-induced gauge fields for ultracold atoms, Rep. Prog. Phys. **77**, 126401 (2014).

[52] A. Eckardt, Colloquium: Atomic quantum gases in periodically driven optical lattices, Rev. Mod. Phys. **89**, 011004 (2017).

[53] M. Boll, T. A. Hilker, G. Salomon, A. Omran, J. Nespolo, L. Pollet, I. Bloch, and C. Gross, Spin-and density-resolved microscopy of antiferromagnetic correlations in Fermi-Hubbard chains, Science **353**, 1257 (2016).

[54] C. A. Regal, M. Greiner, and D. S. Jin, Observation of resonance condensation of fermionic atom pairs, Phys. Rev. Lett. **92**, 040403 (2004).

[55] M. Aidelsburger, M. Atala, M. Lohse, J. T. Barreiro, B. Paredes, and I. Bloch, Realization of the Hofstadter Hamiltonian with ultracold atoms in optical lattices, Phys. Rev. Lett. **111**, 185301 (2013).

[56] S. Moudgalya, N. Regnault, and B. A. Bernevig, η-pairing in Hubbard models: From spectrum generating algebras to quantum many-body scars, Phys. Rev. B **102**, 085140 (2020).

[57] C. Weitenberg and J. Simonet, Tailoring quantum gases by Floquet engineering, Nat. Phys. **17**, 1342 (2021).

[58] M. Müller, S. Diehl, G. Pupillo, and P. Zoller, Engineered open systems and quantum simulations with atoms and ions, Adv. At. Mol. Opt. Phys. **61**, 1 (2012).

[59] P. M. Harrington, E. J. Mueller, and K. W. Murch, Engineered dissipation for quantum information science, Nat. Rev. Phys. **4**, 660 (2022).

[60] S. Dutta, N. Cooper, and S. Kuhr, Data and code to generate all figures for "Generating symmetry-protected long-range entanglement," Apollo – University of Cambridge Repository, 2024, DOI: 10.17863/CAM.105623.

[61] T. Shi, E. Demler, and J. I. Cirac, Variational study of fermionic and bosonic systems with non-Gaussian states: Theory and applications, Ann. Phys. **390**, 245 (2018).

[62] M. Kormos, Inhomogeneous quenches in the transverse field ising chain: scaling and front dynamics, SciPost Phys. **3**, 020 (2017).

[63] Y. Y. Atas, E. Bogomolny, O. Giraud, and G. Roux, Distribution of the ratio of consecutive level spacings in random matrix ensembles, Phys. Rev. Lett. **110**, 084101 (2013).

[64] V. Oganesyan and D. A. Huse, Localization of interacting fermions at high temperature, Phys. Rev. B **75**, 155111 (2007).

[65] S. Trotzky, P. Cheinet, S. Fölling, M. Feld, U. Schnorrberger, A. M. Rey, A. Polkovnikov, E. A. Demler, M. D. Lukin, and I. Bloch, Time-resolved observation and control of superexchange interactions with ultracold atoms in optical lattices, Science **319**, 295 (2008).

[66] W. Magnus, On the exponential solution of differential equations for a linear operator, Commun. Pure Appl. Math. **7**, 649 (1954).

[67] H. J. Carmichael, *Statistical Methods in Quantum Optics 1: Master Equations and Fokker-Planck Equations* (Springer, Berlin, 1999).